Supplementary Information

Correlative dual-color dSTORM/AFM reveals protein clusters at the cytoplasmic side of human bronchial epithelium membranes

Lulu Zhou,[a,b] Jing Gao,[a] Huili Wang,[a] Yan Shi,[a] Haijiao Xu,[a,b] Qiuyan Yan,[a] Yingying Jing,[a,d] Junguang Jiang,[a] Mingjun Cai*,[a,d] and Hongda Wang*,[a,c,d]

[a] *State Key Laboratory of Electroanalytical Chemistry, Changchun Institute of Applied Chemistry, Chinese Academy of Sciences, Changchun, Jilin 130022, China.*
E-mail: hdwang@ciac.ac.cn
[b] *University of Chinese Academy of Sciences, Beijing 100049, China.*
[c] *Laboratory for Marine Biology and biotechnology, Qing dao National Laboratory for Marine Science and Technology, Qingdao, Shandong 266237, China.*
[d] *University of Science and Technology of China, Hefei, Anhui 230027, China.*

Methods

1. Cell culture

The 16HBE cell line (human bronchial epithelium) was purchased from the Shanghai Institute of Biological Sciences (Shanghai, China). Cells were cultured in RPMI 1640 medium (BI) supplemented with 10% fetal bovine serum (FBS, Gibco), 100 U/ml penicillin and 100 μg/ml streptomycin (BI). Cells were maintained at 37℃ in a humidified atmosphere with 5% CO_2 and passaged every two to three days.

2. Antibody labelling

Monoclonal antibodies (Na^+/K^+-ATPase α, sc-48345 and ankyrin G, sc-12719, Santa Cruz) were labeled with photoswitchable fluorophores (Alexa647 or Alexa532, Invitrogen) as depicted in protocol[1]. Briefly, Alexa647 and Na^+/K^+-ATPase α were mixed at 5:1 ratio of amount of substance in PBS including 0.1 M $NaHCO_3$. The reaction was performed for 1 hour at room temperature in the dark. The labeled antibodies were purified by Illustra NAP-5 column (GE Healthcare). The ratio of dye to antibody was about 1 as determined by absorption spectroscopy. Ankyrin G was similarly labeled with Alexa532.

3. Preparation of F-actin

F-actin was polymerized from G-actin as the manufacturer's protocol (BK003, Cytoskeleton, Inc.).

Briefly, we diluted a G-actin aliquot (10 mg/ml, 5 μl) to 1 mg/ml by adding 45 μl general actin buffer. Then, the G-actin was polymerized by adding 5 μl of 10× actin polymerization buffer and incubated at room temperature for 2 h. The F-actin stock is stable for about 1 month at 4℃.

For AFM imaging only, F-actin samples were prepared as follows. We initially diluted the F-actin stock to 10 μg/ml by adding buffer A (2 mM $MgCl_2$, 1 mM EGTA, 20 mM imidazole-HCl, pH 7.6). Then, we deposited 200 μl of the diluent on APTES-coverslip for 5 min. Afterwards, the excess F-actin was removed by washing with buffer A. Finally, F-actin samples were imaged in buffer A including 1 mM ATP to help stabilize the filaments.

For dSTORM imaging only, F-actin was attached to APTES-coverslip as above. Then, we fixed samples for 15 min in 2% (w/v) glutaraldehyde in buffer A, and treated samples for 7 min with freshly prepared 0.1% (w/v) $NaBH_4$ to reduce background fluorescence resulted from glutaraldehyde fixation. Afterwards, samples were blocked for 15 min in 4% (w/v) bovine serum albumin (BSA) in buffer A and labeled with phalloidin-Alexa647 (A22287, Invitrogen) for ~ 1 h at room temperature in the dark. To remove nonspecific labelling, samples were washed 3 times with buffer A. Finally, samples were imaged in imaging buffer. This buffer contained 50 mM Tris-HCl (pH 7.5), 10 mM NaCl, 10% (w/v) glucose, 0.5 mg/ml glucose oxidase (Sigma-Aldrich), 40 μg/ml catalase (Sigma-Aldrich) and 1% (v/v) β-mercaptoethanol.

For correlative imaging, samples were prepared as dSTORM imaging only. Given sample degrading after dSTORM imaging and fluorescence quenching caused by AFM imaging,[2] AFM imaging was before dSTORM imaging to ensure sample integrity and before fluorescence labelling to avoid fluorescence quenching.

4. Preparation of the cytoplasmic side of HBE membranes

We prepared the cytoplasmic side of cell membranes as depicted else.[3, 4] To ensure cells attached to coverslip tightly, we incubated the detached cells on APTES-coverslips for 15 min and then cultured cells in medium for two days. After two-day growing, cells attached to coverslip were used to prepare the cytoplasmic side of membranes as follows. As shown in Fig. S1, cells were firstly incubated in ice cold PBS containing 2 mM EGTA for 2 min to separate the tight junctions;[5] then, cells were washed with PBS (150 mM, pH 7.5) and incubated in hypotonic PBS buffer (7.5 mM, pH 7.5) for 3 min on ice; afterwards, the cells were sheared open by a rapid stream of 8 ml of the hypotonic buffer through a needle at an angle of 20°. To remove the membrane skeletons, the prepared membranes were incubated in low-salt buffer (6.85 mM NaCl, 0.135 mM KCl, 0.075 mM KH_2PO_4, and 0.405 mM $Na_2HPO_4{\cdot}12H_2O$, pH 7.2) for 10 min on ice. Finally, the cytoplasmic side of membranes were washed with PBS and stored in PBS at 4℃.

For AFM imaging, the prepared membranes were immediately imaged in PBS. For dSTORM imaging, the prepared membranes were initially fixed in 1% (w/v) paraformaldehyde (PFA) for 15

min and washed with PBS three times. Then, the membranes were blocked in PBS adding 4% (w/v) BSA for 30 min. Afterwards, cell membranes were labelled with dyes (for single-color dSTORM, with Alexa647-linked anti-NKA or Alexa532-linked anti-AnkG; for dual-color dSTORM, simultaneously with Alexa647-linked anti-NKA and Alexa532-linked anti-AnkG) for ~ 1 h at room temperature in the dark and washed with PBS three times to remove excess dyes. Finally, samples were incubated in PBS containing 100-nm TetraSpeck microspheres (Invitrogen) for 5 min, washed with PBS and imaged in imaging buffer. For correlative imaging, the cell membranes were prepared as dSTORM imaging, and imaging sequence was the same as F-actin.

5. Labelling the intact HBE cell for dSTORM imaging

To investigate the spatial distribution of AnkG at the cytoplasmic side of the basal membrane of intact HBE cells, we prepared samples as follows. Before dSTORM imaging, HBE cells were cultured on clean coverslips to achieve ~ 50% confluence. Then, the cultured cells were washed twice with PBS and fixed in 4% (w/v) PFA for 10 min. To label AnkG proteins on the intact cells, fixed cells were firstly blocked with a solution of 3% (w/v) BSA and 0.05% (w/v) Triton X-100 in PBS for 2 min, then, stained with Alexa532-linked anti-AnkG in 3% (w/v) BSA in PBS for ~ 1 h at room temperature in the dark, and subsequently rinsed with PBS three times. Afterwards, samples were incubated with multi-color microspheres in PBS for 5 min that served as fiducial markers. Finally, the intact cells were imaged in dSTORM imaging buffer.

6. Random distribution experiment

To obtain the correlation arising from the multiple localizations of individual probes, we needed to conduct the random distribution experiment. For this purpose, the sample was prepared as depicted else[6, 7]. The APTES-coverslip were incubated with a solution of 10 nM Alexa647-linked anti-NKA and 5 μM BSA in PBS for 30 min at room temperature in a humid chamber. Then, the coverslip was washed thoroughly with PBS to remove the unreacted proteins and incubated with 100-nm TetraSpeck microspheres in PBS for 5 min. Finally, the prepared sample was imaged in dSTORM imaging buffer to provide the random distribution and thus to provide correlation arising from the multiple appearance of each protein.

7. Image acquisition on correlative dSTORM/AFM microscopy

The correlative dSTORM/AFM microscopy was built by integrating an AFM 5500 (Agilent Technologies, USA) and an inverted Ti-E microscope (Nikon, Japan). For AFM imaging, topographic images were recorded in acoustic AC mode using oxide-sharpened Si3N4 probes (DNP-S, Veeco, USA) with a nominal spring constant of 0.06 N/m at a scanning speed of 1.5 Hz. All the images were recorded as 512 × 512 pixels using PicoView 1.12 software (Agilent Technologies, USA). AFM data was processed and analyzed with Gwyddion.[8]

dSTORM imaging was conducted under TIRF illumination with an oil-immersion objective (100×, 1.49 NA, Nikon, Japan), appropriate optical filters (dichroic: ZT405/488/532/640rpc-XT; emission filter: ZET532/640m, Chroma) and an EMCCD camera (iXon Ultra 888, Andor). For single-color imaging, samples were excited with a 640-nm (or 532-nm) laser (~2 kW/cm^2), and concurrently activated with a 405-nm laser (0-1 W/cm^2). Dual-color imaging was similar to single-color imaging except that samples were sequentially excited with a 640-nm laser (for Alexa647) and a 532-nm laser (Alexa532). For dual-color imaging, the two wavelength channels were further filtered by band pass filters: FF01-559/34 (Semrock) in the short wavelength channel and ET700/75m (Chroma) in the long wavelength channel. In this study, we recorded 10,000 frames with a 20-ms exposure time and an EM gain of 300 to reconstruct super-resolution images. During the acquisition time, z-drift was eliminated by a focus lock; for F-actin, the lateral drift was corrected using cross-correlation methods; and for intact HBE cells, prepared cell membranes, as well as random distribution experiment, multi-color microspheres were embedded as fiducial markers to correct the lateral drift and to calibrate chromatic aberration for dual-color imaging.

Raw image sequences were processed with ThunderSTORM software,[9] which determine sub-diffraction localizations by fitting a suitable PSF model using maximum-likelihood estimation. To reject localizations too dim or too wide, we only considered localizations with a precision below 30 nm, and a photon count more than 100. Besides, localizations appearing in consecutive frames within a distance of 20 nm were merged into a single localization. The reconstructed dSTORM images were viewed based on an average shifted histogram approach.

8. dSTORM data analysis

To analyze the distributions of NKA and AnkG at the cytoplasmic side of cell membranes, three algorithms, hierarchical single-emitter hypothesis test (H-SET),[10, 11] ripley's K function[12] and density-based spatial clustering of applications with noise (DBSCAN)[13] were used.

H-SET is a top-down hierarchical clustering algorithm.[10, 11] The aim of H-SET is to correct over-counting effect of observations (localizations) in raw dSTORM data resulted from multiple observations of individual fluorophores. To this end, we make a null hypothesis (all observations are from the same fluorophore) which is not rejected if the p value (the probability that N observations come from a single fluorophore, where N is the number of observations) is larger than the level of significance (LoS = 0.01 was used). The p value is calculated using the log-likelihood ratio statistic R.

$$R = -2\,log\left(L / L_0\right)$$

where L is the likelihood of the N observations, given a fluorophore located at the maximum likelihood position and given the observation uncertainties, and L_0 is the likelihood of the N

positions, assuming there are N independent fluorophores. In M dimensions, R is chi-squared distributed with M(N-1) degrees of freedom. The maximum likelihood position stated above is the variance-weighted mean value of the N observations.

$$\bar{X} = \frac{\sum_{i=1}^{N} \frac{X_i}{(\sigma_i')^2}}{\sum_{i=1}^{N} \frac{1}{(\sigma_i')^2}} \text{ where } (\sigma_i')^2 = \sigma_i^2 + \sigma_{reg}^2$$

where X_i and σ_i are coordinate and uncertainty of the observation i, respectively; σ_{reg} is the registration error, and σ_i' is the modified uncertainty including the effect of drift correction. The uncertainty in the maximum likelihood position is then calculated from the variance of the weighted mean:

$$\bar{\sigma}^{-2} = \frac{1}{\sum_{i=1}^{N} \frac{1}{(\sigma_i')^2}}$$

The algorithm H-SET proceeds in two passes. For pass 1 of H-SET, we use the MATLAB standard hierarchical clustering algorithm (linkage) to connect observations in clusters from top to bottom, and then test whether observations in individual clusters come from a point source. If yes ($p > LoS$), observations in cluster are collapsed into a single localization; if no ($p \leq LoS$), we iterate the above step. For pass 2 of H-SET, we use a known clustering algorithm such as DBSCAN to identify clusters of localizations from pass 1, and then check whether localizations in individual clusters come from a point source as pass 1. Depending on two parameters: the maximum distance between two points in a cluster (ε) and the minimum number of points to make a cluster (minPts), clusters can be identified with DBSCAN. Given that we can detect spurious clusters in a random distribution once the localization density is high enough, the two parameters ε and minPts should be optimized to satisfy two requirements: minimizing the detection of spurious clusters in random simulated data and sensitively detecting clusters in experimental data. To determine the optimal ε and minPts for our experiment (NKA and AnkG in HBE membrane) in pass 2 of H-SET, we firstly changed the values for ε and minPts (20-40 nm and 5-15, respectively) and computed the corresponding number of multi-clusters (with over three molecules), N_{multi}, which was respectively averaged over all the ROIs for experimental (8 ROIs in 4 NKA images) and simulated random data (25 ROIs); then we compared N_{multi} in the two data to acquire the biggest difference of N_{multi}, satisfying the above two requirements and thus obtained the optimal ε and minPts (22 nm and 5, respectively). Fig. S4 showed maps of N_{multi} as a function of ε and minPts for experimental data, random simulated data and their difference.

Ripley's K analysis is an ensemble measurement of local spatial distribution. The linear transformation of K(r), L(r) – r, was calculated as following equations to interpret the spatial

randomness: the amplitude of L(r) − r is expected to be zero for randomly distributed points and positive for clustering points.

$$K(r) = \frac{A}{n^2} \sum_{i=1}^{n} \sum_{j=1}^{n} \delta_{ij} \text{ where } \delta_{ij} = 1 \text{ if } d_{ij} < r \text{ , otherwise 0}$$

$$L(r) = \sqrt{K(r) / \pi}$$

where A is the area of the analyzed region, n is the number of points, r is the radius for the K-function calculation and d_{ij} is the distance between points i and j.

DBSCAN emphasizes a local measure of clustering. It identifies individual clusters according to two parameters ε and minPts. In our analysis, ε was set to 50 nm and a minimum of 3 localizations was used to define a cluster. Using DBSCAN, we extracted specific cluster information including cluster diameter, cluster density (cluster number per unit area), cluster ratio (dividing the number of proteins in the clusters by the total number of proteins) and protein number in cluster. All statistical data relating to cluster properties were derived from more than 10 cell membranes in 5 independent experiments. All these analyses were performed using H-SET[11] and SuperCluster[14], custom programs written in MATLAB. Codes are accessible at http://stmc.health.unm.edu/tools-and-data/index.html.

To evaluate the potential bias arising from clustering analysis, we compared the distribution of NKA at the cytoplasmic side of cell membranes quantified by H-SET with that by pair-correlation analysis (PCA)[6, 7, 15]. In the PCA algorithm, the pair auto-correlation function g(r) is measured by Fast Fourier Transforms, and then fitted to an appropriate model to extract parameters that could be used to quantify the nano-organization of proteins. Because correlation function g(r) quantifies the increased probability of finding another localized signal at a distance r away from a given localized signal compared to that expected from random distribution, the equation of g(r) can be described as follow.

$$\begin{aligned} g(r)^{measured} &= g(r=0) * g(r)^{psf} + g(r>0) * g(r)^{psf} \\ &= \exp(-r^2 / 4\sigma^2) / (4\pi\sigma^2\rho) + g(r>0) * g(r)^{psf} \end{aligned} \quad (1)$$

The first term of equation (1), referred to as $g(r)^{stoch}$, represents the stochastic correlation arising from multiple appearances of single protein. The second term of equation (1), referred to as $g(r)^{protein}$, represents the contribution from relative spatial position of the protein molecules. In the special case of random distribution of labelled molecules, the protein correlation function $g(r)^{protein}$ is equal to 1. Thus, the total measured correlation function can be represented by:

$$g(r)^{measured} = \exp(-r^2 / 4\sigma^2) / (4\pi\sigma^2\rho) + 1 \quad (2)$$

where σ is the standard deviation of the effective PSF and ρ is the average density of the protein that can be calculated by $\rho = \rho^{loc} / \alpha$ (ρ^{loc} is the average localzation density, and α is the

average number of localizations of single molecule). From the random distribution, we could evaluate $g(r)^{stoch}$ by using the parameters σ and α. In our random distribution experiment, we measured parameters σ and α to be 19.5 nm and 34, respectively. For clustered distribution, the protein correlation function $g(r)^{protein}$ is fitted to an exponential form of $g(r>0)*g(r)^{psf} = 1 + A\exp(-r/\xi)$. Thus, measured correlation takes the following form:

$$g(r)^{measured} = \exp(-r^2/4\sigma^2)/(4\pi\sigma^2\rho) + A\exp(-r/\xi) + 1 \qquad (3)$$

where ξ is the correlation length (an estimate of cluster radius) and A is a measure of the protein density in cluster. To correct the over-counting effect on the distribution of proteins, $g(r)^{protein}$ is calculated by subtracting $g(r)^{stoch}$ from the total measured autocorrelation $g(r)^{measured}$. Here, $g(r)^{stoch}$ is computed by $\alpha * g(r)^{psf}/\rho^{loc}$, and the values α and $g(r)^{psf}$ can be acquired from the random distribution experiment. Besides, the average number of proteins per cluster can be calculated by: $N^{cluster} = 2A\pi\xi^2\rho$. We also performed PCA in MATLAB, and the code are accessible at http://stmc.health.unm.edu/tools-and-data/index.html.

9. Coordinate-based colocalization (CBC)

To quantify the degree of colocalization between NKA and AnkG at the cytoplasmic side of cell membranes, the CBC analysis,[16] a robust method to derive colocalization information from dSTORM data, was employed. We firstly selected same regions (2 μm × 2 μm) from dual-color dSTORM data whose chromatic aberration was corrected in advance, and then calculated the CBC value (C_A) using colocalization function in ThunderSTORM. C_A is range from -1 to 1 (perfect colocalization for $C_A = 1$, colocalization for $0 < C_A < 1$, no colocalization for $C_A = 0$, and segregated but near localizations for $-1 < C_A < 0$).

10. Overlay between AFM and dSTORM

According to matching algorithm between AFM and STORM images described elsewhere,[2] we edited a custom MATLAB program with a Graphical User Interface (GUI) to achieve registration between AFM and dSTORM images. The image matching algorithm is depicted as follows. Considering various aberrations involved in AFM and dSTORM imaging and dSTORM image usually containing a larger field of view than the AFM image, the net effect of these is approximated as an affine transformation of dSTORM localizations and the transformation parameters are estimated by optimizing the overlap between the structures in AFM and dSTORM images. The 2D affine transformation is described as

$$x' = Ax + By + T_x$$
$$y' = Cx + Dy + T_y$$

where x and y are original coordinates (dSTORM localizations), x' and y' are post-transformed coordinates, A, B, C and D are lumped parameters which can cause rotation, scale and shear

operations, and T_x and T_y are translation parameters. According to the sum of the post-transformed dSTORM localizations with a signal in the corresponding area of the AFM image, the optimization of overlay between AFM and dSTORM images is conducted.

11. Performance of correlative dSTORM/AFM microscopy

We used in vitro polymerized F-actin as a model to test the performance of correlative microscopy setup. As shown in Fig. S7, the AFM image of F-actin in panel A showed a single filament with an average height of 7.5 nm and width of 15 nm; the dSTORM image in panel B showed the distribution of the specific labelled F-actin from which we could distinguish two adjacent actin filaments with widths of 22 nm and 33 nm. Comparing with the diameter (8 nm) of a single F-actin filament measured by electron microscopy,[17] we thus confirmed that the correlative microscopy was able to offer high-quality AFM image with the lateral resolution of ~ 10-20 nm and vertical resolurion of ~ 0.1 nm, as well as dSTORM image with the resolution of ~ 20 nm.

12. Image registration for correlative images of cell membranes

To deepen insight into the membrane compartmentation, localizing specific labelled proteins within the high-resolution topography of cell membranes is indispensable. However, features in high-resolution membrane topography are not obvious, which makes it difficult to achieve image registration between high-resolution AFM and dSTORM. We thus aligned low-resolution AFM with dSTORM, and then achieved registration between high-resolution AFM and dSTORM through the correlation between low- and high-resolution AFM. To estimate the registration precision, we used F-actin, with known filamentous structure, as reference sample. As shown in Fig. S8, registration for the correlative images of F-actin was performed and displayed. For the recorded AFM images: low-resolution (AFM_{low}) and high-resolution (AFM_{high}), we extracted F-actin structure via setting the substrate height as threshold and then matched the two images based on cross-correlation function. The merged image in Fig. S8C showed a strong correlation between AFM_{low} and AFM_{high}. For registration between AFM_{low} and dSTORM, we aligned F-actin structure in AFM_{low} image with that in dSTORM image through an accurate affine transformation of dSTORM localizations. From the merged image in Fig. S8D, we also observed good overlay between AFM_{low} and dSTORM. Thus, AFM_{high} and corresponding region in AFM_{low} (ROI_{low}) were

well matched with the corresponding magnified dSTORM image (ROI_{sto}),respectively (Fig. S8E and S8F).

To estimate the extent of registration for the correlative images of F-actin, we determined the following values: number of dSTORM localizations (N), area (A), as well as localization density (D = N/A), occurring at the substrate (h = 0) and F-actin (h > 0) for both ROI_{low}/ROI_{sto} and AFM_{high}/ROI_{sto} images. As shown in Fig. S9A, all the above values in ROI_{low}/ROI_{sto} were almost equal to those in AFM_{high}/ROI_{sto}, which further demonstrated the good registration between AFM_{low} and AFM_{high}. For the slight difference, we attributed to the difference of pixel area in AFM_{low} and AFM_{high}. From the histogram for localization density in Fig. S9A, we also found that the probability for dSTORM localizations occurring at F-actin was 8 times higher than that at substrate, verifying the good overlay between AFM (including AFM_{low} and AFM_{high}) and dSTORM. To measure the registration precision, we cropped F-actin with the same height distribution from merged AFM_{high}/ROI_{sto} image and then compared the AFM height of F-actin with the height at which dSTORM localizations preferred to occur. Fig. S9B showed the three regions we cropped and the corresponding correlative images of F-actin. The height profiles in Fig. S9C indicated that the AFM heights of F-actin in regions 1-3 were ~ 10 nm, ~18 nm and ~16 nm, respectively. The distributions of localization density for regions 1-3 suggested dSTORM localizations had the maximum probability of occurrence at heights of ~ 9 nm, ~ 14 nm, and ~ 14.5 nm, respectively (Fig. S9D). Taken together, the precision of registration between AFM_{high} and dSTORM was demonstrated to be below 10 nm. Thus, for correlative images of cell membranes, the precision for localizing specific proteins within the high-resolution topography of cell membranes can be achieved below 10 nm if the low-resolution AFM image can be matched well with the high-resolution AFM and dSTORM images, respectively.

For evaluation the registration for correlative images of cell membranes, the alignment of low-resolution AFM and corresponding dual-color dSTORM images, as well as the correlation between AFM_{low} and AFM_{high} needed to be analyzed, respectively. Fig. S10 showed an example for the alignment of low-resolution AFM and corresponding dual-color dSTORM images of cell membrane. For such alignment, we needed to perform two steps in advance, one was extracting the whole membrane structure in AFM_{low} as shown in Fig. S10A, the other was correcting chromatic aberration of the dual-color dSTORM images as shown in Fig. S10B and S10C; then, the

overlap between membrane structures in AFM_{low} and dual-color dSTORM images was optimized by synchronously transformation of the dual-color dSTORM localizations, as shown in Fig. S10D. To evaluate the registration of AFM_{low} and dual-color dSTORM, localization densities of NKA and AnkG occurring at the substrate (h = 0) and cell membrane (h > 0) were measured, respectively. Fig. S10E showed that both NKA and AnkG preferred occurring at the region of the cell membrane rather than the substrate, indicating the good registration of AFM_{low} and dual-color dSTORM. To further verify the above result, we showed another example for the alignment of AFM_{low} and dual-color dSTORM (Fig. 5). The magnified views shown in Fig. 5E clearly revealed that AnkG proteins were perfectly localized on the membrane marginal structure, cilia. We thus confirmed that dual-color dSTORM images of NKA and AnkG could be well aligned with the low-resolution AFM image of the cell membrane.

Then, we analyzed the correlation between AFM_{low} and AFM_{high} of cell membranes. As shown in Fig. S11A-S11C, the topographical images displayed the structure and organization of the cytoplasmic side of cell membrane from whole to local and from low resolution to high resolution. Because features of AFM_{high} in AFM_{low} were not obvious, we introduced a corresponding medium-resolution image (AFM_{medium}) to match AFM_{low} with AFM_{high}. Fig. S11E showed an almost perfect colocalization between AFM_{high} and the corresponding region in AFM_{medium} (ROI_{medium}); Fig. S11D also showed a strong colocalization between AFM_{medium} and the corresponding region in AFM_{low} (ROI_{low}); thus, the above results demostrated the good alignment between AFM_{high} and AFM_{low}. Taken together, we demonstrated that localizing specific proteins NKA and AnkG within the high-resolution AFM image of the cell membrane could be achieved with precision below 10 nm by aligning dual-color dSTORM with AFM_{low} and correlating AFM_{high} with AFM_{low}.

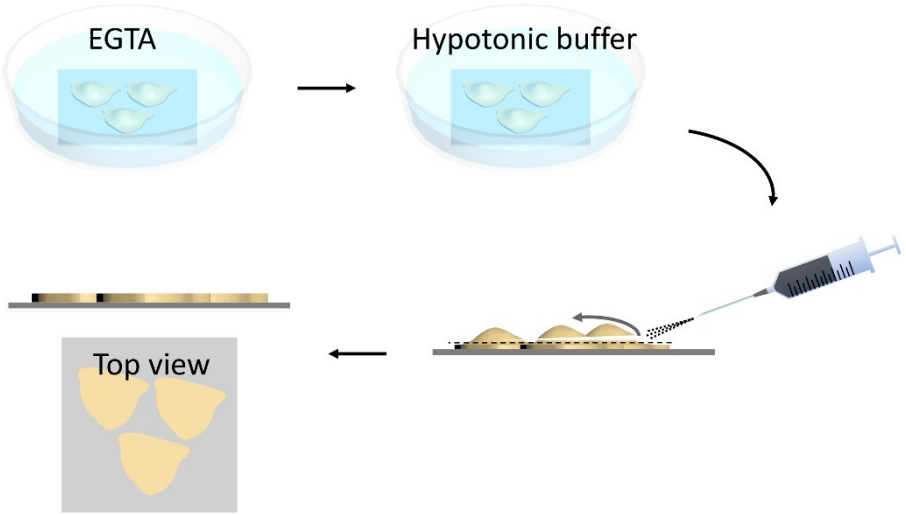

Figure S1. The workflow of preparing the cytoplasmic side of cell membranes. Cells were sequentially incubated in ice cold EGTA to separate the tight junctions and in hypotonic PBS buffer for 3 min on ice. Then, intact cells were sheared open by a fast stream of hypotonic buffer, and thus the cytoplasmic side of cell membranes were exposed on the coverslip.

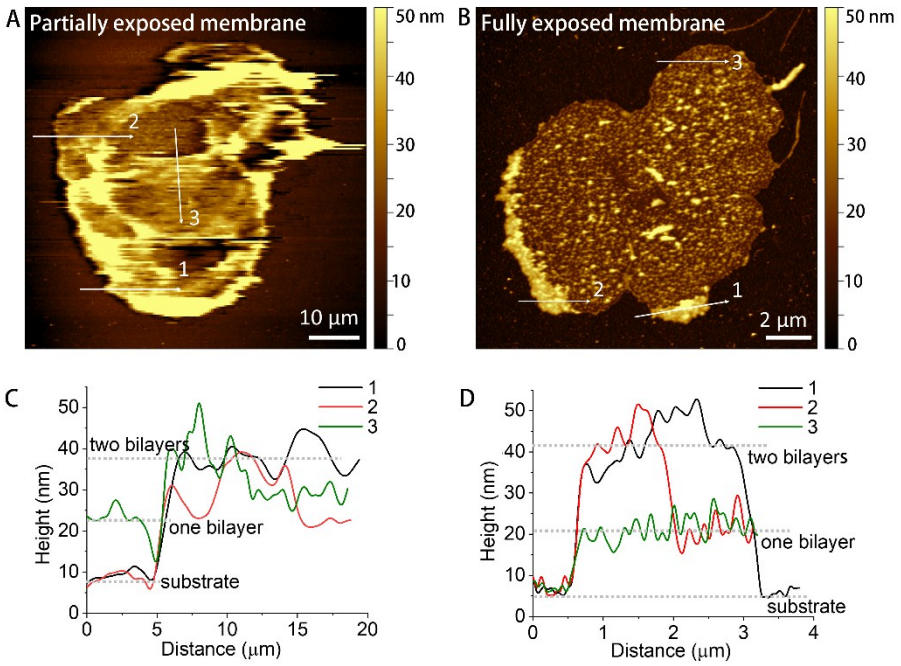

Figure S2. Recognition of the partially and fully exposed membranes. (A, B) Topographic images of partially (A) and fully (B) exposed membranes. (C, D) Height profiles corresponding to lines in (A, B).

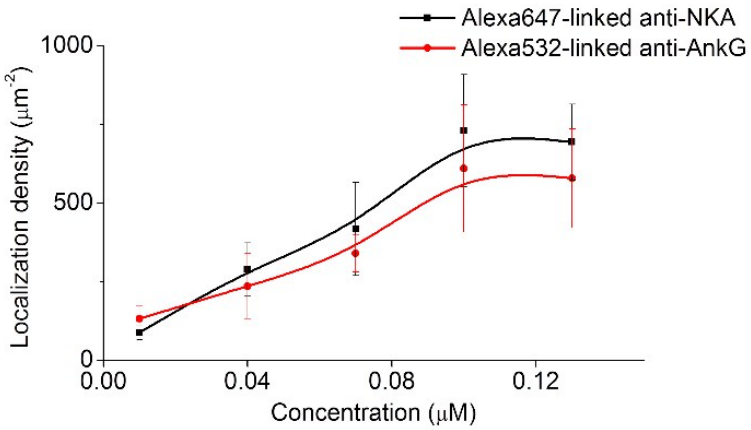

Figure S3. The saturated labelling concentration of Alexa647-linked anti-NKA and Alexa532-linked anti-AnkG for the cytoplasmic side of the HBE membrane. The plot of localization density at five labelling concentrations (0.01, 0.04, 0.07, 0.1, 0.13 μM) show that the saturated concentration is ~0.10 μM. Symbols and errors represent the means and SD, respectively. The data are obtained from ten membranes at each concentration.

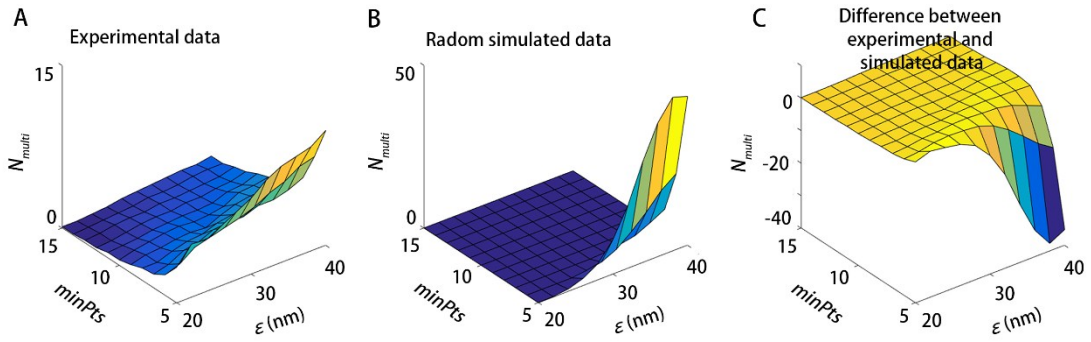

Figure S4. Parameter optimization for pass 2 of H-SET. (A-C) 3D maps of N_{multi} as a function of ε and minPts for experimental data (A), random simulated data (B) and the difference (C).

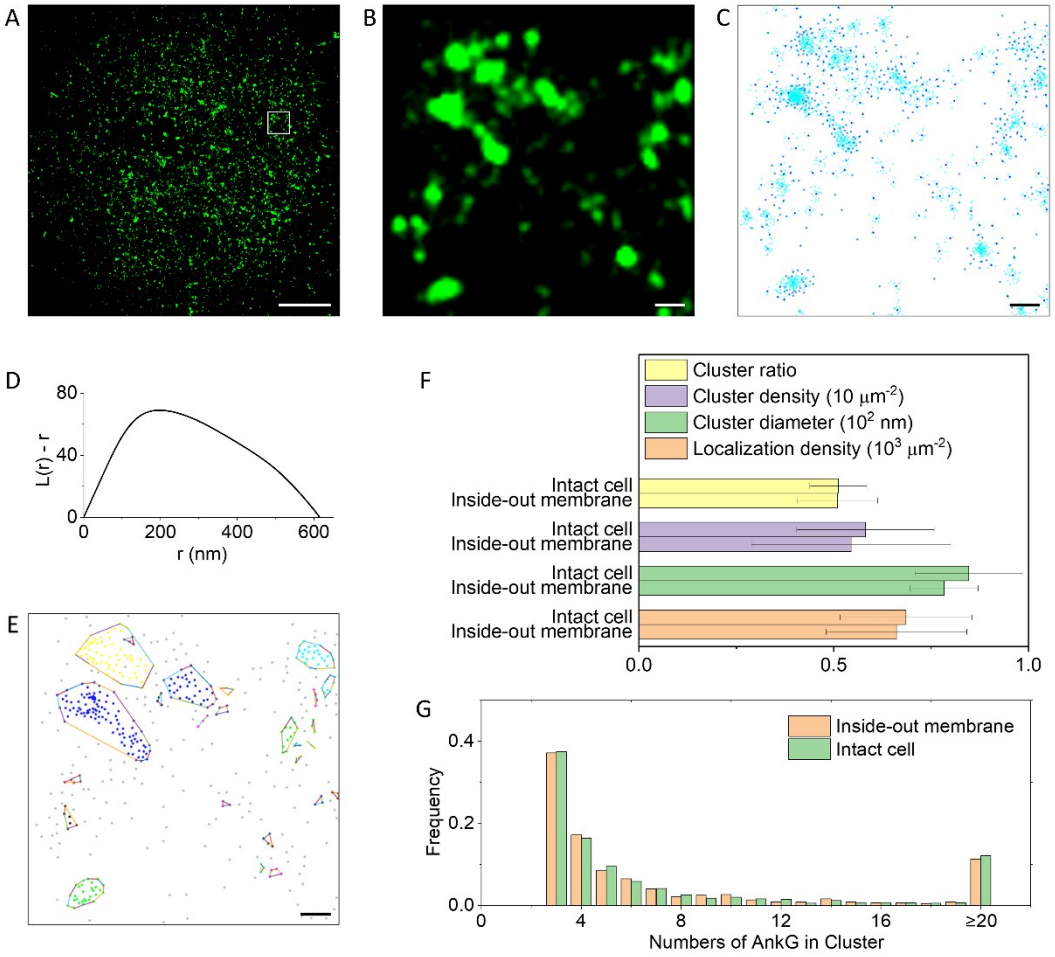

Figure S5. Distribution of AnkG at the cytoplasmic side of the basal membrane of intact HBE cells. (A) dSTORM image of AnkG stained with Alexa532-linked anti-AnkG. (B) Magnified view of region in white of (A). (C) Scatter plot of AnkG corresponding to (B). Cyan dots indicate observations (localizations) in raw data, and blue dots indicates locations (localizations) after correcting over-counting effect by H-SET. (D) Ripley's K function analysis of AnkG locations after H-SET. (E) DBSCAN cluster map of AnkG locations after H-SET. (F, G) Comparing characteristics of the distribution of AnkG proteins at the cytoplasmic side of the basal membrane of intact cells with those at the cytoplasmic side of prepared membranes. Error bars represent the standard deviation of the mean of over 10 intact cells or inside-out membranes. Scale bars: 5 μm (A) and 200 nm (B, C, E).

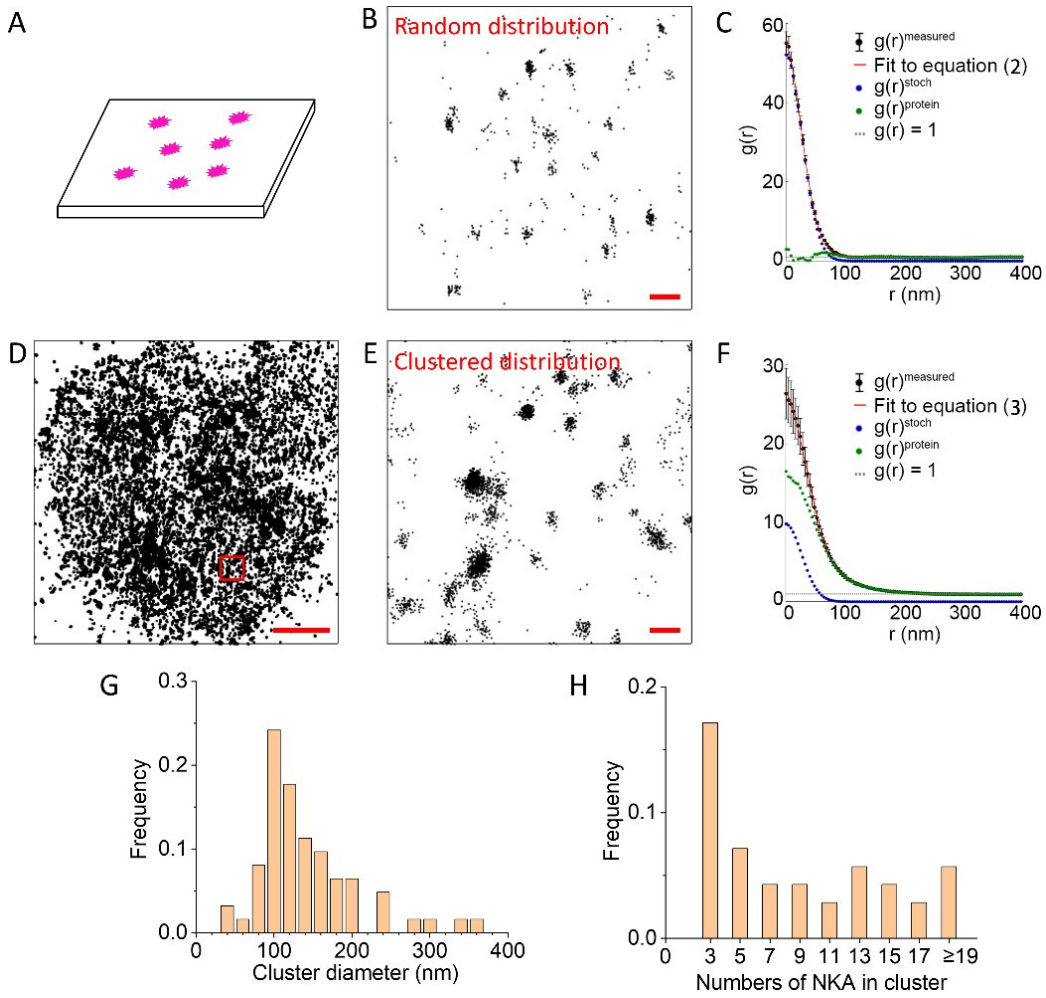

Figure S6. Pair-correlation analysis of the distribution of NKA proteins at the cytoplasmic side of cell membranes. (A) Diagram showing Alexa647-linked anti-NKA molecules randomly immobilized on an APTES-coverslip. (B) Distribution of Alexa647-linked anti-NKA molecules in a 2 μm × 2 μm region on the coverslip. (C) Plot of measured auto-correlation function $g(r)^{measured}$ of Alexa647-linked anti-NKA molecules on the coverslip. The correlation function is an average over 50 distinct regions on the coverslip, and error bars represent the standard error of the mean. $g(r)^{measured}$ is well fitted to equation (2) with parameters σ = 19.5 nm for the standard deviation of the effective PSF and α = 34 for the average number of localizations of individual Alexa647-linked anti-NKA molecules. (D) Distribution of NKA proteins at the cytoplasmic side of cell membranes. (E) Magnified view of a 2 μm × 2 μm region in red of (D). (F) Correlation function of NKA proteins averaged 16 inside-out cell membranes. Error bars on black points represent the standard error of the mean of the 16 membranes. $g(r)^{measured}$ is well fitted to equation (3) with parameters: ξ = 61 nm, A = 7.8, σ = 26.5 nm and ρ = 6.3 μm^{-2}, and the average surface density of labelled molecules is ~ 21.5 μm^{-2}, which indicates that NKA proteins tend to form small clusters. (G, H) Cluster diameter (G) and proteins per cluster (H) revealed by pair-correlation analysis. Data are from 80 regions with areas of 4 μm^2. Scale bars: 200 nm (B, E), 5 μm (D).

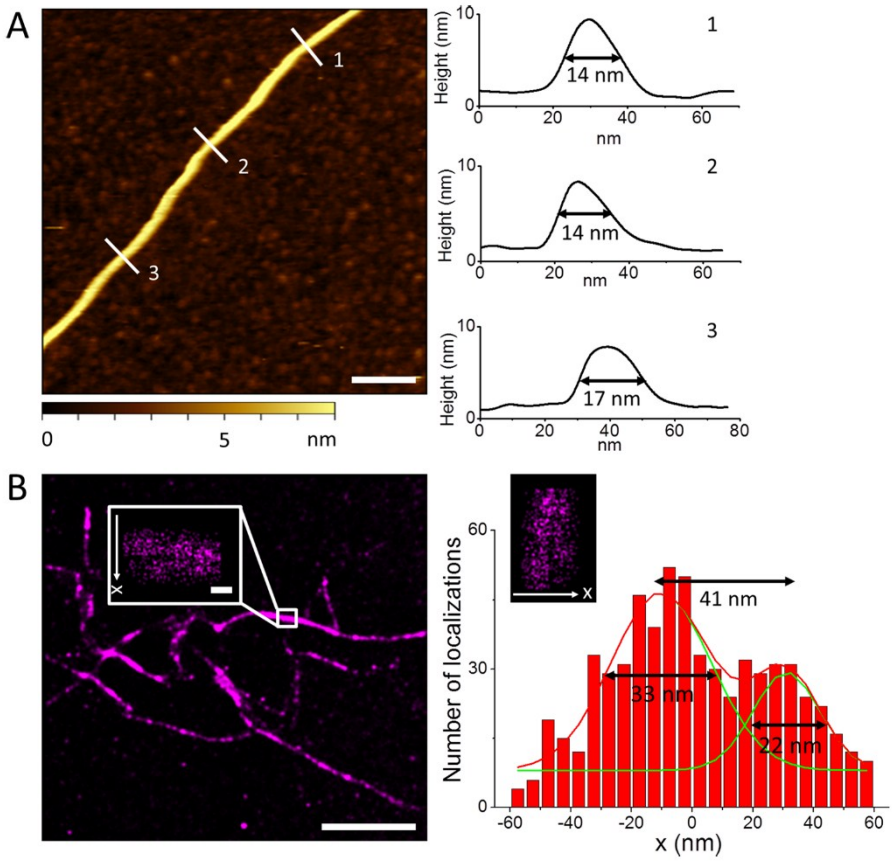

Figure S7. The performance of correlative dSTORM/AFM microscopy. (A) AFM image of F-actin attached on APTES-coverslip. Profiles 1, 2 and 3 show the height along the line 1, 2 and 3 which are perpendicular to the F-actin. (B) dSTORM image of F-actin stained with phalloidin-Alexa647. The inset is the magnified image of the selected white box. The cross-sectional profile of adjacent F-actin filaments in the inset is shown in the right panel. Scale bars: 100 nm (A), 2 μm (B), 50 nm (inset).

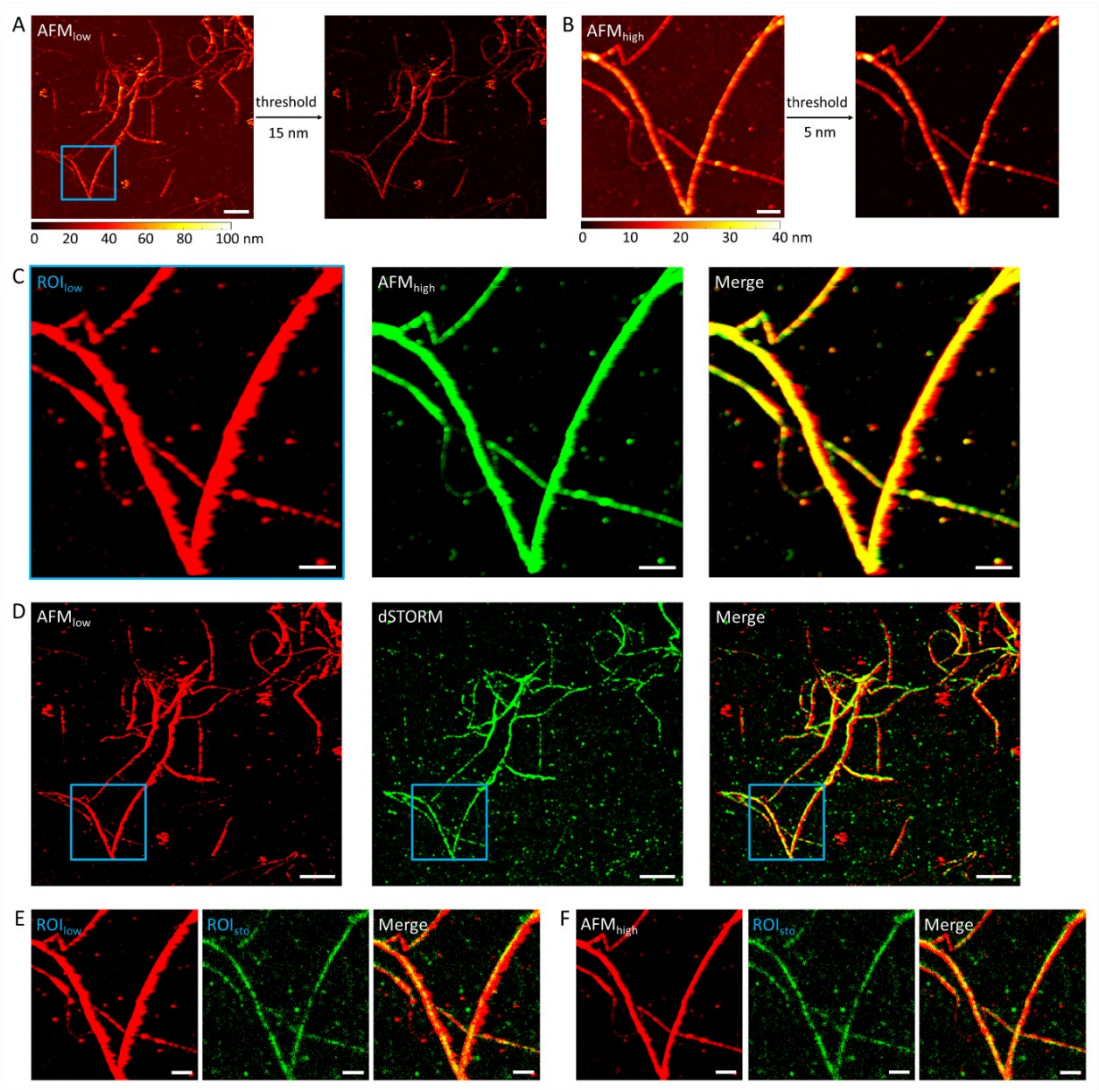

Figure S8. An example of F-actin to show the alignment process. (A, B) Setting a threshold to distinguish F-actin structure from the substrate. Based on the substrate height, the threshold for low-resolution AFM (AFM_{low}) is set as 15 nm, and 5 nm for high-resolution AFM (AFM_{high}). The light blue box in (A) shows the region (ROI_{low}) of AFM_{high} in AFM_{low}. (C) Overlay between AFM_{high} and ROI_{low}. The merged image suggests the good overlay between AFM_{high} and AFM_{low}. (D) Image registration between dSTORM and AFM_{low} images. According to the F-actin structure, the dSTORM localizations are processed with affine transformation to achieve accurate overlay with AFM_{low}. The light blue boxes indicate the region of AFM_{high} in AFM_{low}. (E, F) ROI_{low} (E) and AFM_{high} (F) separately merging with corresponding region of dSTORM (ROI_{sto}). Scale bars: 2 μm (A, D) and 500 nm (B, C, E and F).

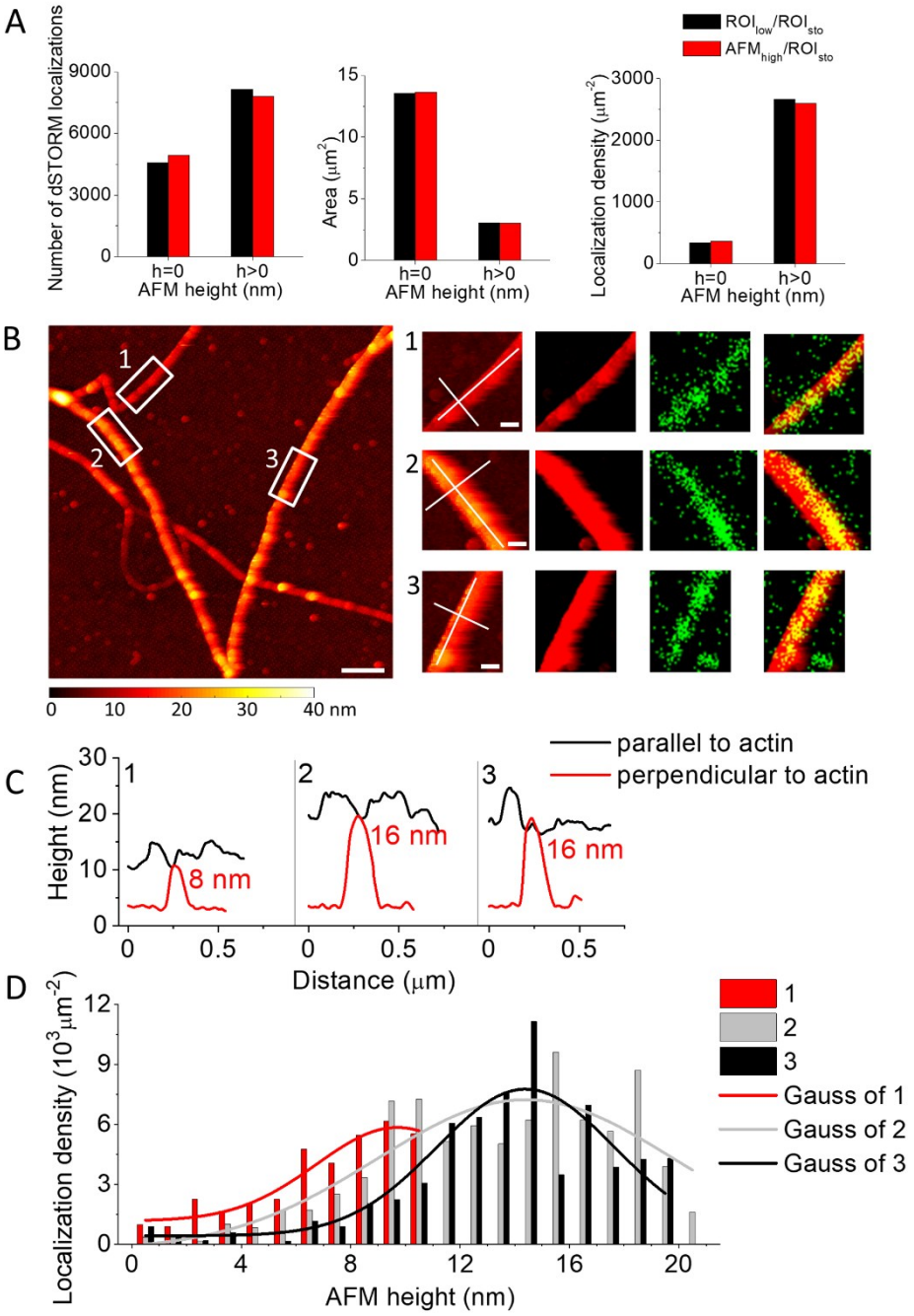

Figure S9. Estimating the registration precision. (A) Histograms showing the number of dSTORM localizations (left), area (middle), and localization density (right) at the substrate (h = 0) and F-actin (h > 0) in merged ROI_{low}/ROI_{sto} and AFM_{high}/ROI_{sto} images. (B) Three selected regions in AFM_{high} image and the corresponding correlative images of F-actin. The scale in AFM_{high} image is 500 nm, and the scale is 100 nm in magnified images. (C) Height plots along actin and perpendicular to actin for the three regions in white boxes of (B). (D) Histogram of localization density versus AFM height in the three regions.

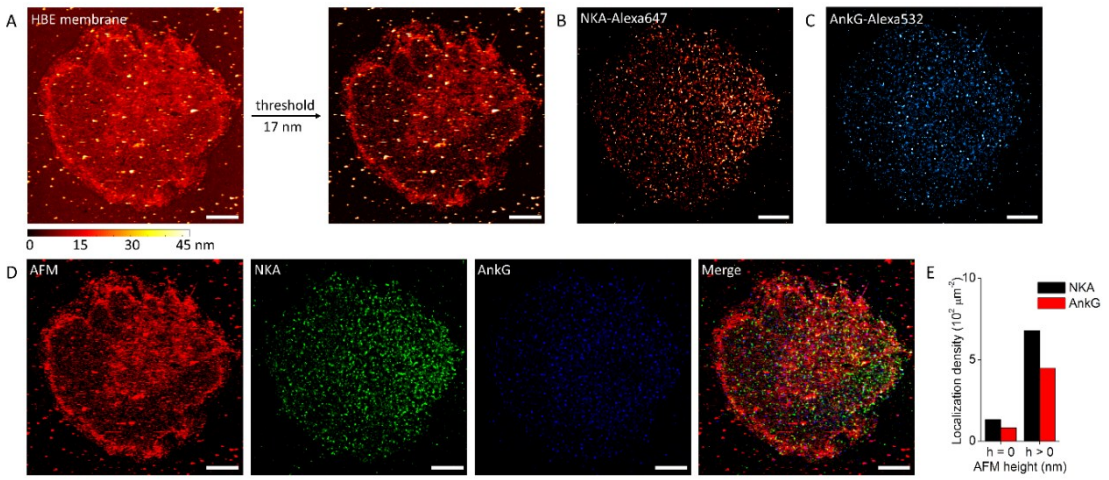

Figure S10. Correlative images of the cytoplasmic side of human bronchial epithelia (HBE) membrane. (A) The topography of the HBE membrane. Through subtracting the height of substrate (17 nm), the HBE membrane structure was extracted. (B, C) Reconstructed dSTORM images showing the distributions of Na^+/K^+-ATPase (NKA) (B) and ankyrin G (AnkG) (C) on the cytoplasmic side of HBE membrane. (D) Registration between AFM and dual-color dSTORM images. (E) Histogram showing the localization density of NKA and AnkG occurring at substrate and HBE membrane. Scale bar: 5 µm (A-D).

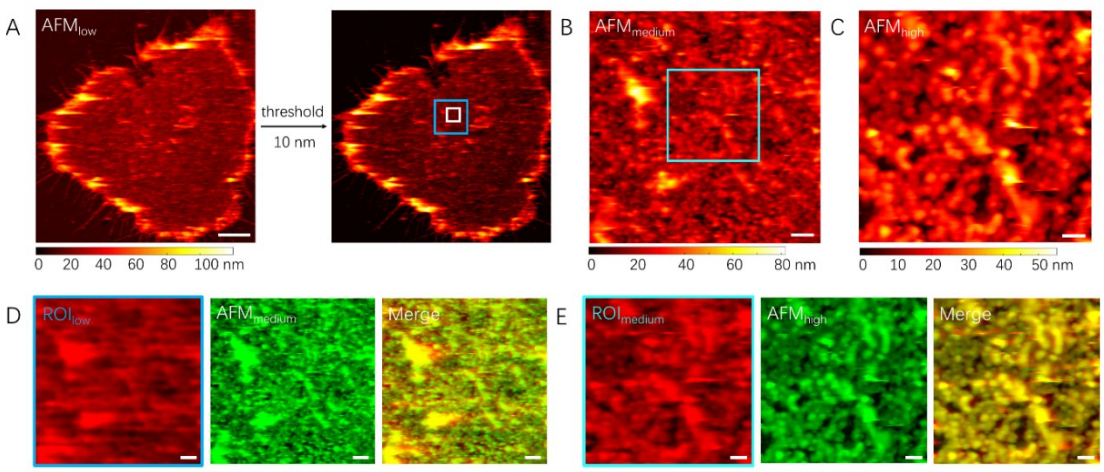

Figure S11. Correlation of low-resolution AFM with high-resolution AFM for the cytoplasmic side of HBE membrane. (A-C) AFM images with resolution from low to high (AFM_{low}, AFM_{medium} and AFM_{high}). For AFM_{low}, we set a threshold, 10 nm, to separate the membrane structure from the substrate. The light blue box in AFM_{low} indicates corresponding AFM_{medium} region (ROI_{low}); and the cyan box in AFM_{medium} indicates corresponding AFM_{high} region (ROI_{medium}). (D, E) Registration between AFM images. Merged images ROI_{low}/AFM_{medium} (D) and ROI_{medium}/AFM_{high} (E) suggest the good overlay between AFM_{high} and AFM_{low}. Scale bars: 5 μm (A), 500 nm (B, D) and 200 nm (C, E).

References:

1. M. Bates, S. A. Jones and X. Zhuang, *Cold Spring Harb. Protoc.*, 2013, **2013**, 540-541.
2. P. D. Odermatt, A. Shivanandan, H. Deschout, R. Jankele, A. P. Nievergelt, L. Feletti, M. W. Davidson, A. Radenovic and G. E. Fantner, *Nano Lett.*, 2015, **15**, 4896-4904.
3. M. Cai and H. Wang, in *Pharmaceutical Nanotechnology: Basic Protocols*, eds. V. Weissig and T. Elbayoumi, Springer New York, New York, NY, 2019, DOI: 10.1007/978-1-4939-9516-5_22, pp. 361-372.
4. Y. Shan and H. Wang, *Chem. Soc. Rev.*, 2015, **44**, 3617-3638.
5. W. J. Nelson and P. J. Veshnock, *J. Cell Biol.*, 1986, **103**, 1751-1765.
6. P. Sengupta, T. Jovanovic-Talisman, D. Skoko, M. Renz, S. L. Veatch and J. Lippincott-Schwartz, *Nat. Methods*, 2011, **8**, 969-975.
7. P. Sengupta, T. Jovanovic-Talisman and J. Lippincott-Schwartz, *Nat. Protoc.*, 2013, **8**, 345-354.
8. D. Necas and P. Klapetek, *Cent. Eur. J. Phys.*, 2012, **10**, 181-188.
9. M. Ovesný, P. Křížek, J. Borkovec, Z. Švindrych and G. M. Hagen, *Bioinformatics*, 2014, **30**, 2389-2390.
10. M. S. Graus, M. J. Wester, D. W. Lowman, D. L. Williams, M. D. Kruppa, C. M. Martinez, J. M. Young, H. C. Pappas, K. A. Lidke and A. K. Neumann, *Cell Reports*, 2018, **24**, 2432-2442.e2435.

11. J. Lin, M. J. Wester, M. S. Graus, K. A. Lidke and A. K. Neumann, *Mol. Biol. Cell*, 2016, **27**, 1002-1014.
12. J. Zhang, K. Leiderman, J. R. Pfeiffer, B. S. Wilson, J. M. Oliver and S. L. Steinberg, *Micron*, 2006, **37**, 14-34.
13. M. Ester, H.-P. Kriegel, J. Sander and X. Xu, 1996.
14. M. S. Itano, M. S. Graus, C. Pehlke, M. J. Wester, P. Liu, K. A. Lidke, N. L. Thompson, K. Jacobson and A. K. Neumann, *Front. Phys.*, 2014, **2**.
15. S. L. Veatch, B. B. Machta, S. A. Shelby, E. N. Chiang, D. A. Holowka and B. A. Baird, *PLoS One*, 2012, **7**, e31457.
16. S. Malkusch, U. Endesfelder, J. Mondry, M. Gelléri, P. J. Verveer and M. Heilemann, *Histochem. Cell Biol.*, 2012, **137**, 1-10.
17. J. Hanson and J. Lowy, *J. Mol. Biol.*, 1963, **6**, 46-60.